Kuwait J.Sci., Vol.49, No.(4),October.2022,pp(1-13)

Synthesis and photocatalytic activity of TiO_2 on phenol degradation

Muhamad D. Permana[1], Atiek R. Noviyanti[1], Putri R. Lestari[2], Nobuhiro Kumada[2], Diana R. Eddy[1,*], Iman Rahayu[1]

[1]*Dept. of Chemistry, Faculty Mathematics and Natural Sciences, Universitas Padjadjaran Sumedang, West Java-45363, Indonesia*

[2]*Center for Crystal Science and Technology, University of Yamanashi Kofu, Yamanashi 400-8511, Japan*

[*]*Corresponding author: diana.rahmawati@unpad.ac.id*

Abstract

Photocatalysis is a process of accelerating reactions that are assisted by energy from light irradiation. Titanium dioxide (TiO_2) is one of the most widely developed photocatalysis materials, and is used because of its high catalytic activity, stability and very affordable. The most commonly used precursors of TiO_2 are titanium butoxide (TBOT) and titanium tetraisopropoxide (TTIP). These variations in precursor can lead to phase difference in the formation of TiO_2 crystals, which further improves its nature in the activity of photocatalysis. In this study, the sol-gel method was used to synthesize titanium dioxide nanoparticles from variations of TBOT and TTIP. Furthermore, the structure, crystallite size and band gap of TiO_2 were determined by X-ray diffraction (XRD) and UV-vis reflectance spectroscopy (DRS). Subsequently, TiO_2 photocatalytic activity was evaluated in phenol photodegradation as a contaminant model with UV irradiation. The results showed the structure synthesized from TBOT had a higher amount of anatase, higher crystallinity, smaller crystallite size, larger band gap, and better photocatalytic activity than those from TTIP. Furthermore, it was shown that TiO_2 from TBOT had an efficiency of 147% greater than TiO_2 P25 Degussa, while TiO_2 from TTIP had 66% efficiency compared to TiO_2 P25.

Keywords: Phenol; photo catalyst; TBOT; TiO_2; TTIP

1. Introduction

Phenols are toxic chemical compounds and they are slowly degraded in the environment to form different aromatic intermediates. In fact, most of them cause environmental hazards (Peiró *et al*., 2001). Nevertheless, this compound and its intermediates can be reduced by various methods, which include photocatalysis (Lestari *et al*., 2021), ozonation (Shahamat *et al*., 2014; Wei *et al*., 2020), adsorption (Miao *et al*., 2013; Zhang *et al*., 2016; Dehmani *et al*., 2020), biological (Pradeep *et al*., 2015), and Fenton methods (Gümüş & Akbal, 2016; Yazdanbakhsh *et al*., 2020). Although the most suitable and widely used method is photocatalysis due to its advantages of

efficient industrial waste degradation (Ameta & Ameta, 2016), affordability, and environmentally friendly (Chong *et al*., 2010).

Titanium dioxide (TiO_2) is an effective photocatalyst and it is applied in various fields such as environmental and energy, including self-cleaning surfaces (Tavares *et al*., 2014; Banerjee *et al*., 2015), air and water purification systems (Turkay & Kumbur, 2019; Mamaghani *et al*., 2020), sterilization (Junkar *et al*., 2016), and photoelectrochemical conversion (Wang *et al*., 2011; Nakata & Fujishima, 2012). The main advantages of this compound include high chemical stability under acidic and basic conditions, non-toxic, affordability, and is an environmentally safe oxidizer, making it potential for many photocatalytic applications (Eddy *et al*., 2018; Alkhayatt *et al*., 2021).

The TiO_2 is divided into 3 main phases namely anatase, rutile, and brookite (Haggerty *et al*., 2017). Generally, anatase has the best photocatalytic ability compared to others because it shows a deeper excited charge carrier in large part leading to a higher surface reaction (Luttrell *et al*., 2014). Heterophase of TiO_2 can effectively stimulate electron transfer from one phase to another which helps to increase its photocatalytic performance (Hu *et al*., 2018; Ding *et al*., 2020). For instance, the well-known TiO_2 P25 Degussa which consists of ~20% rutile and ~80% anatase, is an exceptionally good photocatalyst (Berger *et al*., 2005).

Most of this compound was synthesized using organometallic precursors such as titanium butoxide (TBOT) (Gan *et al*., 2018; Wang *et al*., 2018; Lendzion-Bieluń *et al*., 2020) and titanium tetraisopropoxide (TTIP) (Cenovar *et al*., 2012; Paunović *et al*., 2015). The inorganic alkoxide precursor is preferred because of its ability to hydrolyze easily to the oxide phase due to its exposure to water (Syoufian *et al*., 2007).

Behnajady *et al*. (2011) investigated the conditions of TiO_2 synthesis using TBOT and TTIP for photocatalysis on the removal of C.I. Acid Red27 (AR27). Niu *et al*. (2014) also reported the synthesis of nanoparticles of this compound by microwave radiation method under difference precursor between $TiCl_4$, $Ti(SO_4)_2$, and TBOT for photocatalytic degradation of methylene blue (MB).

Cenovar *et al*. (2012) reported that they have successfully synthesized TiO_2 using the sol-gel method from TTIP. The results showed anatase had a stable crystal structure within the temperature range of 250 - 650°C. Zhao *et al*. (2009) reported a tested and proven effective method to synthesize brookite TiO_2 which is using hydrothermal methods or reflux conditions from the TBOT precursor. The results showed crystal structure of pure anatase, pure brookite, and brookite/anatase mixtures were formed.

However, there has been no report showing comparison in the effect of TBOT and TTIP precursors on TiO_2 crystal properties and their activity on phenol degradation. In this study, the compound was synthesized by sol-gel method from organometallic TBOT and TTIP. The effect of these parameters was further investigated on the crystal phase, size, lattice parameters, band gap energy, and its photocatalytic activity in phenol degradation.

2. Materials and methods

2.1 Materials

The materials used in this study were ethanol (C_2H_5OH, 99%, Merck), phenol (C_6H_5OH, 99%, Merck), TiO_2 nanoparticles (P25 Degussa, 20% rutile and 80% anatase, Merck), titanium butoxide (TBOT, $Ti(OC_4H_9)_4$, 99%, Sigma Aldrich), and titanium tetraisopropoxide (TTIP, $Ti(OC_3H_7)_4$, 99%, Sigma Aldrich). All ingredients were used without treatment.

2.2 Synthesis of TiO_2

Ethanol 95 mL and 0.48 mL of distilled water were mixed together and stirred for 30 mins, then a TiO_2 precursor (1.5 mL TBOT or 2.0 mL TTIP) in 18 mL ethanol was injected into the mixture at a rate of 0.5 mL/min using a syringe pump. After injection, the temperature was raised to 85°C under reflux at a stirring speed of 900 rpm for 100 mins. Furthermore, the precipitate was isolated by centrifugation, washed with distilled water and ethanol, dried in vacuum, and calcined at 800℃ for 2 hours in the air to obtain TiO_2 TBOT (representing TiO_2 synthesized from the precursor TBOT) and TiO_2 TTIP (representing TiO_2 synthesized from the precursor TTIP).

2.3 Characterization of TiO_2

X-ray diffraction (XRD) patterns were obtained on a Rigaku/MiniFlex 600, and then measured at room temperature with Cu Kα radiation (λ = 1.5418 Å). The scan ranged from 20 to 80 (2θ). Also, the crystallite size was determined by using the Debye-Scherrer equation (Eddy *et al*. 2020):

$$B = K\lambda / D \cos \quad (1)$$

Where D is the crystal size, K is the Scherrer constant (0.9), λ is the wavelength of the X-ray radiation, B is the value of the peak FWHM (full width at half maximum), and θ is the angle of diffraction.

Crystallinity was calculated by comparing the crystalline peak (I_c) with the total (crystalline peak (I_c) and amorphous peak (I_a)).

$$\text{Crystallinity (\%)} = I_c / (I_c+I_a) \times 100\% \quad (2)$$

A Jasco V-550 spectroscopy was used to record the UV-visible (UV-vis) spectra, and the analysis range was from 200 to 800 nm. The optical band gap energy (E_g) was obtained using the Tauc equation:

$$(\alpha h\nu)^{1/n} = A(h\nu - E_g) \quad (3)$$

where α is the absorption coefficient, hν is photon energy, and A is the proportionality constant. Furthermore, the transition property is represented by n, where n = 2 for the indirect band gap allowed (Chowdhury *et al*. 2019).

2.4 Photocatalytic Analysis

Photocatalytic degradation was carried out with 50 mL of a 20 mg/L phenol solution with 15 mg catalyst, within a period of 60 mins under dark adsorption (no irradiation source). Subsequently, the mixture was stirred at 300 rpm for 2 hours under light irradiation (300 W Xe lamp, UV ray with wavelength <390 nm, PE300BUV) at a distance of 150 mm above the surface of the solution. Furthermore, the time was tested to determine the remaining phenol concentration using reverse-phase high-performance liquid chromatography (HPLC, Jasco Co-2065Plus), with UV detector (Jasco UV-2075Plus), C-18 column or Octadecyl Silica (ODS) as the stationary phase and a mixture of distilled water and methanol as the mobile phase. The HPLC used methanol:water (1:1) as eluent, with a column temperature of 40°C and a column flow rate of 1.00 mL/min (Lestari *et al*., 2020).

The equation below was used to calculate the percentage of phenol adsorption and degradation:

$$\% \text{ Removing} = (C_i - C_t) / C_i \times 100\% \quad (4)$$

Where C_i is the initial phenol concentration and C_t is phenol concentration at time t.

The kinetics of photocatalysis were calculated using first and second-order models. The first-order kinetics were calculated (Eddy *et al*., 2020):

$$\ln(C_t/C_i) = -k_1 t + b \quad (5)$$

Where, C_i denotes the initial phenol concentration ($mg.L^{-1}$), C_t is the phenol concentration ($mg.L^{-1}$) in solution at t mins, b denotes the constant, and k_1 (min^{-1}) is the first-order rate constant. Then a second-order kinetics model was calculated based on the rate obtained from square of the number of sites on the catalyst surface (Turki *et al*., 2015). The equation after integration is obtained as:

$$1/C_t - 1/C_i = -k_2 t + b \quad (6)$$

Where, k_2 denotes the second-order rate constant ($L.mol^{-1}.min^{-1}$).

3. Result and discussion

3.1 Characterization of Photocatalyst

3.1.1 X-ray diffraction Analysis

The results of X-ray diffraction (XRD) analysis are shown in Figure 1. The XRD patterns of P25, TiO_2 TBOT, and TiO_2 TTIP showed similarity with the Inorganic Crystal Structure Database (ICSD) 98-017-2914 for anatase (tetragonal, space group $I4_1/amd$) and ICSD 98-016-7961 for

rutile (tetragonal, space group $P4_2/mmm$). The highest peak of P25 was attained at 2θ = 25.27°, while the highest peak of TiO_2 TBOT was observed at 2θ = 25.25°, and the highest peak of TiO_2 TTIP was at 2θ = 27.38°. Also, P25 and TiO_2 TBOT had the highest peaks in relation to the anatase at 2θ = 25.30°, while TiO_2 TTIP had the highest peaks in relation to rutile at 2θ = 27.43°.

TiO_2 P25 Degussa crystals showed peak pattern at 2θ = 25.3° (011), 37.8° (004), 48.0° (020), 53.9° (015), 55.0° (121), 62.7° (024), 68.8° (116), 70.3° (220), and 75.1° (125) in the crystalline plane of anatase. In addition, the peaks at 27.4° (110) and 36.1° (011) were obtained from the rutile phase plane. For TiO_2 TBOT, there were additional peaks at 41.23° (111) and 44.04° (120) which were considered to be from the rutile phase. This was also observed in TiO_2 TTIP at 41.23° (111), 44.04° (120), 54,31° (121), 56.62° (220), and 68.99° (031), and is considered to have been derived from the rutile phase.

Table 1. Percentage of anatase and rutile phase in photocatalysts.

Photocatalysts	Phase (%)	
	Anatase	Rutile
TiO_2 P25	85.7	14.3
TiO_2 TBOT	33.2	66.8
TiO_2 TTIP	0.9	99.1

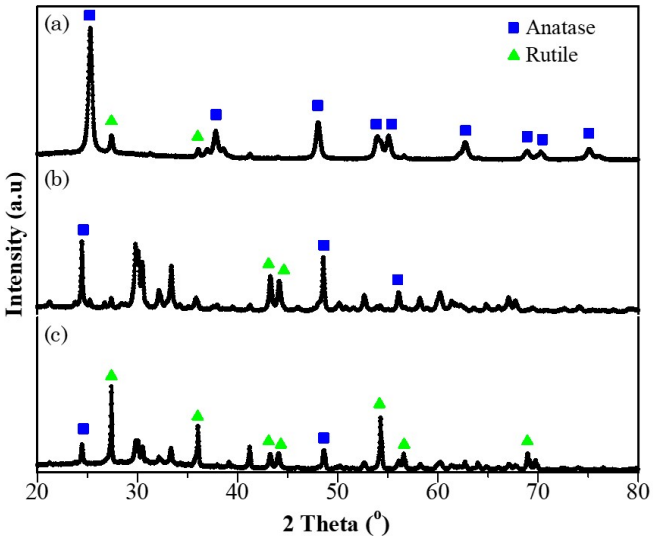

Fig. 1. XRD pattern of photocatalyst (a) P25, (b) TiO_2 TBOT, and (c) TiO_2 TTIP.

A Rietveld refinement of the TiO_2 sample was performed from the XRD pattern. The percentage of TiO_2 phase is shown in Table 1. At the same calcination temperature (800°C), TiO_2 TBOT had a higher anatase percentage (33.2%) than TiO_2 TTIP (0.9%). This showed that different precursors require different energy to form its crystal lattice. These results can be compared to Behnajady *et al*. (2011) which stated that TiO_2 synthesized through the TBOT precursor produced a higher percentage of anatase than TiO_2 from TTIP.

Table 2 shows the crystallinity and crystallite size of photocatalysts. It shows that the synthesis from TBOT and TTIP precursors have a higher crystallinity than TiO_2 P25 Degussa. Meanwhile, high crystallinity is required in photocatalysis because of its ability to prevent the possibility of electron-hole recombination, in order to increase photocatalytic activity (Zheng *et al*. 2018). However, those from TBOT have higher crystallinity than those from TTIP which can support photocatalysis.

The crystallite size of the synthesized TiO_2 showed a larger size than Degussa TiO_2 P25 in anatase and rutile. This result was possible due to the sol-gel method which increased the crystallite size. However, those from the TBOT showed smaller size in anatase (75.28 nm) than those from the TTIP (81.44 nm). Also, in the rutile phase, TiO_2 from TBOT showed a larger size (73.37 nm) than TiO_2 from TTIP (52.23 nm).

Table 2. The crystallinity and crystallite size of photocatalysts.

Photocatalysts	Crystallinity (%)	Crystallite size (nm)	
		Anatase	Rutile
TiO_2 P25	46.01	32.84	22.59
TiO_2 TBOT	75.67	75.28	73.37
TiO_2 TTIP	60.57	81.44	52.23

Table 3. The crystal lattice parameters of photocatalysts.

Photocatalyst	Anatase			Rutile		
	a=*b* (Å)	*c* (Å)	V(Å^3)	*a*=*b* (Å)	*c* (Å)	V(Å^3)
ICSD 98-017-2914	3.78	9.51	136,27	-	-	-
ICSD 98-016-7961	-	-	-	4.59	2.96	62.47
TiO_2 P25	3.78	9.50	136.11	4.59	2.96	62.32
TiO_2 TBOT	3.78	9.50	135.89	4.59	2.96	62.38
TiO_2 TTIP	3.73	9.37	130.36	4.59	2.96	62.42

Table 4. The band gap of photocatalysts.

Photocatalysts	Wavelength (nm)	Band gap (eV)
TiO_2 P25	411.9	3.01
TiO_2 TBOT	414.7	2.99
TiO_2 TTIP	439.7	2.82

Table 3 shows the lattice parameters of TiO_2, and is seen that the synthesized substance has anatase crystals with a smaller lattice than TiO_2 P25 Degussa. Furthermore, those from the TTIP have smaller lattice than those from the TBOT with a crystal lattice volume of 135.8914 Å^3 for TiO_2 TBOT and 130.3639 Å^3 for TiO_2 TTIP. Whereas in rutile crystals, the synthesized substance showed a larger lattice than TiO_2 P25 Degussa. A comparison of the precursor

synthesis was also done, and it was observed that those of TTIP have larger lattice with a volume of 62.4220 $Å^3$ compared to TBOT, with a crystal lattice volume of 62.3819 $Å^3$. This shows that synthesizing this compound by sol-gel method can decrease the anatase crystal lattice and increase rutile. This effect occurs more in synthesis from TTIP precursors than those from TBOT.

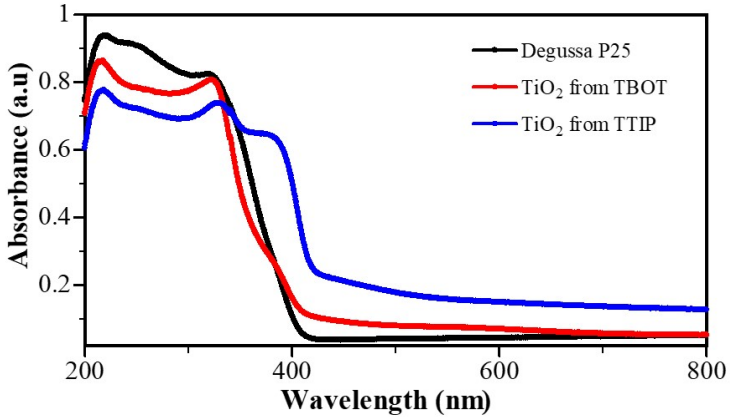

Fig. 2. Photocatalysts absorbtion in range 200-800 nm.

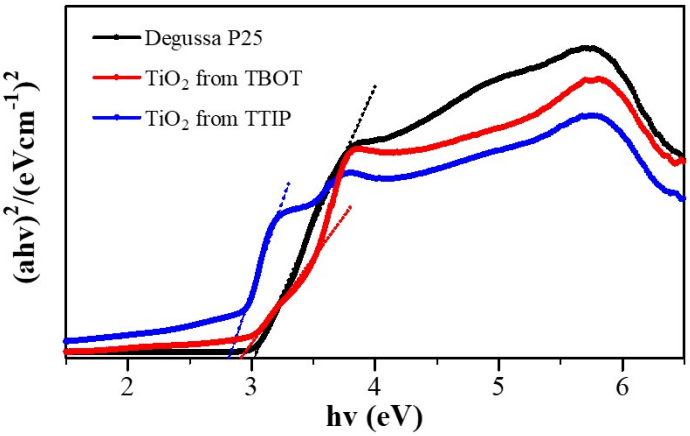

Fig. 3. The band gap of a photocatalysts using Tauc equation.

3.1.2 UV-vis Spectroscopy Analysis

The UV-vis absorption spectrum is shown in Figure 2. TiO_2 P25 Degussa has clear ultraviolet light absorption characteristics and does not absorb visible light. However, those synthesized from the TTIP has absorption characteristics that extends from 350 nm to 413 nm, and attain its maximum absorption at 385 nm. The red shift of TiO_2 uptake from TBOT and TiO_2 from TTIP compared to TiO_2 P25 Degussa showed there was a decrease in the band gap for the synthesized TiO_2.

Band gap energy is calculated by plotting $(\alpha h\nu)^2$ vs $h\nu$ (Figure 3). The values for P25, TiO_2 from TBOT, and TiO_2 from TTIP are shown in Table 4. Therefore, it is seen that the synthesized TiO_2 causes a slight decrease in band gap than P25 Degussa. This is due to the formation of rutile phase, which is more dominant than anatase, where the standard anatase has a band gap of 3.2

eV and rutile has 3.0 eV (Luttrell *et al*. 2014). In addition, TiO_2 from TTIP has a smaller band gap value (2.82 eV) because it has a more rutile phase than TiO_2 from TBOT (2.99 eV). The values determined in this work are all smaller than those reported in other literatures.

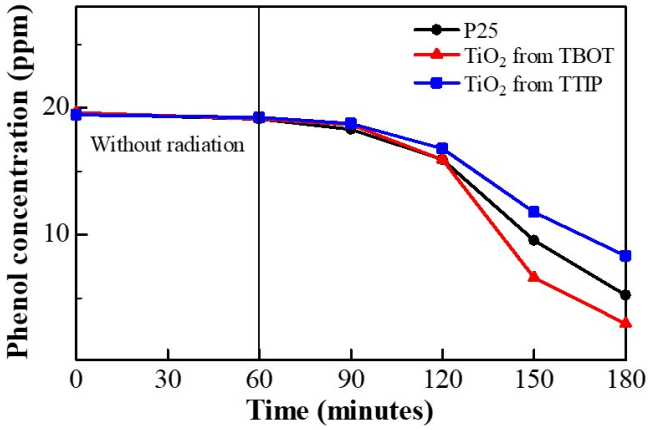

Fig. 4. Photocatalytic activity of catalyst on phenol. The experiment was conducted using 50 mL phenol solution 20 mg/L and 15 mg catalyst with 180 min treatment.

Table 5. The percentage efficiency of phenol adsorption and degradation.

Photocatalysts	Phenol adsorption (%)	Phenol degradation (%)
TiO_2 P25	2.04	71.15
TiO_2 TBOT	2.46	82.38
TiO_2 TTIP	1.04	56.14

Also, variations in the band gap value can be influenced by differences in the crystal lattice parameters. This causes changes of electron density in the crystal (Barajas-Aguilar *et al*., 2018), therefore, the band gap value can be changed.

3.2 Photocatalytic Activity

Experimental results of the photocatalytic degradation of phenol are shown in Figure 4. The activity of photocatalysts exposed to UV rays has better percentage degradation when compared to those not exposed. This showed photons from UV light have a positive effect on photocatalyst performance in phenol oxidation.

Table 5 shows the percentage adsorption and degradation of phenol by photocatalysts. It can be seen that TiO_2 from the TBOT had the largest percentage of adsorption (2.46%) which correlates with the largest percentage of degradation (82.38%). In contrast, those from TTIP have the lowest percentage of adsorption (1.04%) and degradation (56.14%) compared to TBOT and P25 Degussa after 2 hours of UV irradiation. This is because TiO_2 from TBOT has the highest crystallinity which reduces the occurrence of recombination (Zheng *et al*. 2018), while the smaller crystallite anatase size increases the photocatalytic ability. Furthermore, it had a greater

percentage of anatase (33.2%) than the other. The presence of this anatase-rutile heterophase enhances the formation of an electron synergistic effect, which effectively stimulates the transfer of electrons from one phase to another (Hu *et al*., 2018; Ding *et al*., 2020). Although its amount of anatase was too low (0.9%), therefore, this effect might not occur.

Table 6 shows the reaction of kinetic rate constant data based on the pseudo first and second-order models. It is seen that the pseudo first-order model gives a better R-value than the second. This implies that the photocatalytic reaction of phenol degradation fits it. Meanwhile, the highest k value is found in TiO_2 from the TBOT precursor in both models, namely with k_1 of 0.0159 min^{-1} in the first-order model and k_2 of 0.0017 $L.mol^{-1}.min^{-1}$ in the second. The k_1 value in the first is followed by Degussa TiO_2 P25 (0.0108 min^{-1}) and TiO_2 TTIP (0.0071 min^{-1}).

Table 6. The kinetic study of photocatalysts.

Sample	Pseudo first-order		Pseudo second-order	
	k_1	R^2	k_2	R^2
TiO_2 P25	0.0108	0.8663	0.0008	0.6651
TiO_2 TBOT	0.0159	0.8505	0.0017	0.6315
TiO_2 TTIP	0.0071	0.8859	0.0004	0.7243

The results showed the efficiency of phenol removal with TiO_2 from TBOT was 147% greater than TiO_2 P25 Degussa for the first-order model, while TiO_2 from TTIP had 66% efficiency compared to TiO_2 P25 Degussa.

4. Conclusions

In this study, the sol-gel method was used to synthesize titanium dioxide from variations of the TBOT and TTIP precursors and tested for photocatalytic activity on phenol. Results show that TBOT makes TiO_2 dominant with the anatase phase. Also, TiO_2 synthesized from TBOT has high crystallinity, small crystallite size, and higher band gap than TiO_2 from TTIP. In addition, TiO_2 synthesized from TBOT precursor has a higher photocatalytic activity than TiO_2 P25 Degussa with greater efficiency of 147%, while that from TTIP has an efficiency of 66%.

ACKNOWLEDGEMENTS

The authors are grateful for the facilities from Universitas Padjadjaran, Indonesia by Academic Leadership Grant (ALG) Prof. Iman Rahayu (ID: 2203/UN6.3.1/PT.00/2022).

References

Alkhayatt, A.H.O., Hussain, S.A. & Muhammad, S.K. (2021) Hydrothermally growth of TiO_2 Nanorods, characterization and annealing temperature effect. Kuwait Journal of Science, **48**(3).

Ameta, R. & Ameta, S.C. (2016) Photocatalysis: principles and applications. CRC Press, Boca Raton.

Banerjee, S., Dionysiou, D.D. & Pillai, S.C. (2015) Self-cleaning applications of TiO_2 by photo-induced hydrophilicity and photocatalysis. Applied Catalysis B: Environmental, **176**: 396-428.

Barajas-Aguilar, A.H., Irwin, J.C., Garay-Tapia, A.M., Schwarz, T., Delgado, F.P., Brodersen, P.M., Prinja, R., Kherani, N. & Sandoval, S.J.J. (2018) Crystalline structure, electronic and lattice-dynamics properties of $NbTe_2$. Scientific Reports, **8**(1): 1-14.

Behnajady, M.A., Eskandarloo, H., Modirshahla, N. & Shokri, M. (2011) Investigation of the effect of sol–gel synthesis variables on structural and photocatalytic properties of TiO_2 nanoparticles. Desalination, **278**(1-3): 10-17

Berger, T., Sterrer, M., Diwald, O., Knözinger, E., Panayotov, D., Thompson, T.L. & Yates, J.T. (2005) Light-induced charge separation in anatase TiO_2 particles. The Journal of Physical Chemistry B, **109**(13): 6061-6068.

Cenovar, A., Paunovic, P., Grozdanov, A., Makreski, P. & Fidanccevska, E. (2012) Preparation of nano-crystalline TiO_2 by Sol-gel method using titanium tetraisopropoxide (TTIP) as a precursor. Advances in Natural Science: Theory & Applications. **1**(2): 133-142.

Chong, M.N., Jin, B., Chow, C.W. & Saint, C. (2010) Recent developments in photocatalytic water treatment technology: a review. Water research, **44**(10): 2997-3027.

Chowdhury, I.H., Roy, M., Kundu, S. & Naskar, M.K. (2019) TiO_2 hollow microspheres impregnated with biogenic gold nanoparticles for the efficient visible light-induced photodegradation of phenol. Journal of Physics and Chemistry of Solids, **129**: 329-339.

Dehmani, Y., Sellaoui, L., Alghamdi, Y., Lainé, J., Badawi, M., Amhoud, A., Bonilla-Petriciolet, A., Lamhasni, T. & Abouarnadasse, S. (2020) Kinetic, thermodynamic and mechanism study of the adsorption of phenol on Moroccan clay. Journal of Molecular Liquids, **312**: 113383.

Ding, L., Yang, S., Liang, Z., Qian, X., Chen, X., Cui, H. & Tian, J. (2020) TiO_2 nanobelts with anatase/rutile heterophase junctions for highly efficient photocatalytic overall water splitting. Journal of Colloid and Interface Science, **567**: 181-189.

Eddy, D.R., Anggraeni, A., Fauzia, R.P., Rahayu, I., Mutalib, A., Firdaus, M.L. & Bahti, H.H. (2018) Gadolinium-Mesoporous Silica as a Potential Magnetic Resonance Imaging Contrast Agents. Oriental Journal of Chemistry, **34**(5): 2603.

Eddy, D.R., Ishmah, S.N., Permana, M.D. & Firdaus, M.L. (2020) Synthesis of Titanium Dioxide/Silicon Dioxide from Beach Sand as Photocatalyst for Cr and Pb Remediation. Catalysts, **10**(11): 1248.

Gan, Y., Wei, Y., Xiong, J. & Cheng, G. (2018) Impact of post-processing modes of precursor on adsorption and photocatalytic capability of mesoporous TiO_2 nanocrystallite aggregates towards ciprofloxacin removal. Chemical Engineering Journal, **349**: 1-16.

Gümüş, D. & Akbal, F. (2016) Comparison of Fenton and electro-Fenton processes for oxidation of phenol. Process Safety and Environmental Protection, **103**: 252-258.

Haggerty, J.E., Schelhas, L.T., Kitchaev, D.A., Mangum, J.S., Garten, L.M., Sun, W., Stone, K.H., Perkins, J.D., Toney, M.F., Ceder, G. & Ginley, D.S. (2017) High-fraction brookite films from amorphous precursors. Scientific Reports, **7**(1): 1-11.

Hu, J., Zhang, S., Cao, Y., Wang, H., Yu, H. & Peng, F. (2018) Novel highly active anatase/rutile TiO_2 photocatalyst with hydrogenated heterophase interface structures for photoelectrochemical water splitting into hydrogen. ACS Sustainable Chemistry & Engineering, **6**(8): 10823-10832.

Junkar, I., Kulkarni, M., Drašler, B., Rugelj, N., Mazare, A., Flašker, A., Drobne, D., Humpolíček, P., Resnik, M., Schmuki, P. & Mozetič, M. (2016) Influence of various sterilization procedures on TiO_2 nanotubes used for biomedical devices. Bioelektrochemistry, **109**: 79-86.

Lendzion-Bieluń, Z., Wojciechowska, A., Grzechulska-Damszel, J., Narkiewicz, U., Śniadecki, Z. & Idzikowski, B. (2020) Effective processes of phenol degradation on Fe_3O_4–TiO_2 nanostructured magnetic photocatalyst. Journal of Physics and Chemistry of Solids, **136**: 109178.

Lestari, P.R., Takei, T. & Kumada, N. (2021) Novel ZnTi/C_3N_4/Ag LDH heterojunction composite for efficient photocatalytic phenol degradation. Journal of Solid State Chemistry, **294**: 121858.

Lestari, P.R., Takei, T., Yanagida, S. & Kumada, N. (2020) Facile and controllable synthesis of Zn-Al layered double hydroxide/silver hybrid by exfoliation process and its plasmonic photocatalytic activity of phenol degradation. Materials Chemistry and Physics, **250**: 122988.

Luttrell, T., Halpegamage, S., Tao, J., Kramer, A., Sutter, E. & Batzill, M. (2014) Why is anatase a better photocatalyst than rutile? -Model studies on epitaxial TiO_2 films. Scientific Reports, **4**(1): 1-8.

Mamaghani, A.H., Haghighat, F. & Lee, C.S. (2020) Role of titanium dioxide (TiO_2) structural design/morphology in photocatalytic air purification. Applied Catalysis B: Environmental, **269**: 118735.

Miao, Q., Tang, Y., Xu, J., Liu, X., Xiao, L. & Chen, Q. (2013) Activated carbon prepared from soybean straw for phenol adsorption. Journal of the Taiwan Institute of Chemical Engineers, **44**(3): 458-465.

Nakata, K. & Fujishima, A. (2012) TiO_2 photocatalysis: Design and applications. Journal of Photochemistry and Photobiology C: Photochemistry Reviews, **13**(3): 169-189.

Niu, J., Yao, B., Peng, C., Zhang, W. & Chen, Y. (2014) Rapid microwave hydrothermal methods synthesis of TiO_2 photocatalysts using different sources of materials. Integrated Ferroelectrics, **152**(1): 163-173.

Paunović, P., Grozdanov, A., Češnovar, A., Makreski, P., Gentile, G., Ranguelov, B. & Fidančevska, E. (2015) Characterization of nanoscaled TiO_2 produced by simplified sol–gel method using organometallic precursor. Journal of Engineering Materials and Technology, **137**(2).

Peiro, A.M., Ayllón, J.A., Peral, J. & Doménech, X. (2001) TiO_2-photocatalyzed degradation of phenol and ortho-substituted phenolic compounds. Applied Catalysis B: Environmental, **30**(3-4): 359-373.

Pradeep, N.V., Anupama, S., Navya, K., Shalini, H.N., Idris, M. & Hampannavar, U.S. (2015) Biological removal of phenol from wastewaters: a mini review. Applied Water Science, **5**(2): 105-112.

Shahamat, Y.D., Farzadkia, M., Nasseri, S., Mahvi, A.H., Gholami, M. & Esrafili, A. (2014) Magnetic heterogeneous catalytic ozonation: a new removal method for phenol in industrial wastewater. Journal of Environmental Health Science and Engineering, **12**(1): 1-12.

Syoufian, A., Inoue, Y., Yada, M. & Nakashima, K. (2007) Preparation of submicrometer-sized titania hollow spheres by templating sulfonated polystyrene latex particles. Materials Letters, **61**(7): 1572-1575.

Tavares, M.T.S., Santos, A.S.F., Santos, I.M.G., Silva, M.R.S., Bomio, M.R.D., Longo, E., Paskocimas, C.A. & Motta, F.V. (2014) TiO_2/PDMS nanocomposites for use on self-cleaning surfaces. Surface and Coatings Technology, **239**: 16-19.

Turkay, G.K. & Kumbur, H. (2019) Investigation of amoxicillin removal from aqueous solution by Fenton and photocatalytic oxidation processes. Kuwait Journal of Science, **46**(2)**.**

Turki, A., Guillard, C., Dappozze, F., Ksibi, Z., Berhault, G. & Kochkar, H. (2015) Phenol photocatalytic degradation over anisotropic TiO_2 nanomaterials: Kinetic study, adsorption isotherms and formal mechanisms. Applied Catalysis B: Environmental, **163**: 404-414.

Wang, G., Wang, H., Ling, Y., Tang, Y., Yang, X., Fitzmorris, R.C., Wang, C., Zhang, J.Z. & Li, Y. (2011) Hydrogen-treated TiO_2 nanowire arrays for photoelectrochemical water splitting. Nano letters, **11**(7): 3026-3033.

Wang, X., Bai, L., Liu, H., Yu, X., Yin, Y. & Gao, C. (2018) A Unique Disintegration–Reassembly Route to Mesoporous Titania Nanocrystalline Hollow Spheres with Enhanced Photocatalytic Activity. Advanced Functional Materials, **28**(2): 1704208.

Wei, X., Shao, S., Ding, X., Jiao, W. & Liu, Y. (2020) Degradation of phenol with heterogeneous catalytic ozonation enhanced by high gravity technology. Journal of Cleaner Production, **248**: 119179.

Yazdanbakhsh, A., Aliyari, A., Sheikhmohammadi, A. & Aghayani, E. (2020) Application of the enhanced sono-photo-Fenton-like process in the presence of persulfate for the simultaneous removal of chromium and phenol from the aqueous solution. Journal of Water Process Engineering, **34**: 101080.

Zhang, D., Huo, P. & Liu, W. (2016) Behavior of phenol adsorption on thermal modified activated carbon. Chinese Journal of Chemical Engineering, **24**(4): 446-452.

Zhao, B., Chen, F., Huang, Q. & Zhang, J. (2009) Brookite TiO_2 nanoflowers. Chemical Communications, (34): 5115-5117.

Zheng, H., Svengren, H., Huang, Z., Yang, Z., Zou, X. & Johnsson, M. (2018) Hollow titania spheres loaded with noble metal nanoparticles for photocatalytic water oxidation. Microporous and Mesoporous Materials, **264**: 147-150.

Submitted: 11/04/2021
Revised: 06/10/2021
Accepted: 20/10/2021
DOI: 10.48129/kjs.13509